Environmental Semeiotics (2009) **2**(1), 1-15
DOI 10.3383/es.2.1.1

Simulation of Ground Motion and Synthetic Seismograms. The 1908 Messina Earthquake.

CARCIONE J. M., GEI D.

Istituto Nazionale di Oceanografia e di Geofisica Sperimentale, Trieste (Italy)
Email corresponding author: jcarcione@inogs.it

Abstract: We design a numerical algorithm for wave simulation in anelastic media in the presence of free surface, which can be used to model seismic waves at the Earth's surface. The modeling simulates 3-D waves by using the Fourier and Chebyshev methods to compute the spatial derivatives along the horizontal and vertical directions, respectively. The stress-strain relation is based on the Kelvin-Voigt mechanical model, which has the advantage of not requiring additional field variables. The model is based on two anelastic parameters and twice the spatial derivatives of the lossless case. The methodology is illustrated by simulating the Messina 1908 earthquake.

Keywords: Seismic waves, simulation, earthquake, Kelvin-Voigt model.

1. INTRODUCTION

Wave modeling is a valuable tool for seismic interpretation and an essential part of inversion algorithms. Problems regarding environmental geophysics, seismic exploration, foundation engineering, earthquake seismology and non-destructive testing (NDT) of materials require the use of full-wave three-dimensional modeling methods. In particular, it is important to model the surface waves (Rayleigh and Love waves) and record the components of the wave field. Moreover, the unconsolidated nature of the shallow layers in many cases requires an anelastic stress-strain relation to model the dissipation of the wave field. An efficient and highly accurate technique is full-wave modeling by using pseudospectral methods (Carcione, 2007; Carcione *et al.*, 2002). The pseudospectral Chebyshev method is not periodic and allows for the incorporation of boundary conditions by using characteristic variables, in particular, free surface conditions at the surface and non-reflecting conditions at the bottom of the mesh. We use the Kelvin-Voigt mechanical model to describe attenuation. It does not require memory variables and only needs the calculation of

additional spatial derivatives and the use of two anelastic parameters compared to four parameters when using other mechanical models, e. g., the Zener model.

We use the described numerical technique to simulate the 1908 Messina earthquake. This is the largest seismic event that had occurred in the southern part of the Calabrian arc since 1983 A.D. (Capuano *et al.*, 1988). It was the most catastrophic earthquake in Italy during this century, with extensive damage and 60,000 people killed according to Baratta (1910) or 120000 casualties according to Mercalli (1909). The duration of the mainshock is reported as approximately 23 s and 110 seismic stations all over the world recorded the event but the original records are virtually unavailable nowadays (Mulargia and Boschi, 1983). It was felt by people in a radius of 300 km from the epicenter with a Mercalli intensity value of XII (Amoruso *et al.*, 2002).

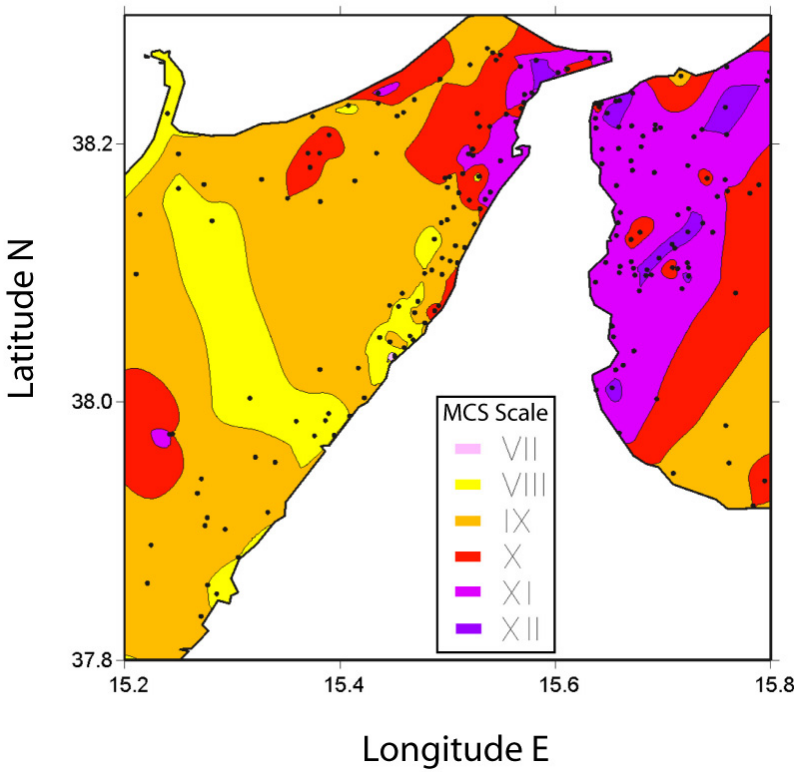

Figure 1: Macroseismic intensity map for the 1908 Messina earthquake. Data from the Catalogo Parametrico dei Terremoti Italiani (CPTI).

This earthquake was followed by a tsunami with sea waves as high as 12 m, entering locally up to 200 m inland (Amoruso *et al.* (2002), Platania (1909)). Smaller earthquakes were felt in the Messina region one month before the main event to ~10 years after (Amoruso *et al.*, 2002). A total of 293 events are reported in the period December 28, 1908 – March 31, 1909; the distribution of aftershocks shows a clear exponential decay (Mulargia and Boschi, 1983). The magnitude of the event can be estimated between M*s* 7.1 (Riuscetti and Schick, 1975) and M*s* 7.5 (Gutenberg and Richter, 1954) because of the low quality of the seismograms, at the dawn of instrumental seismology, and the complexity of the source (Boschi *et al.*, 1989).

Catastrophical damages spread out over an area of 4300 km^2. Figure 1 shows a macroseismic intensity map of the study area. Data come from the Catalogo Parametrico dei Terremoti Italiani (CPTI).

2. THE NUMERICAL MODELLING TECHNIQUE

2.1 The 3D equation of motion

The three-dimensional equations of momentum conservation can be expressed as:

$$\rho \ddot{u}_i = \frac{\partial \sigma_{ij}}{\partial x_j}, \tag{1}$$

where ρ is the density, u_i are the displacement component and σ_{ij} denote the stress components. A dot above a variable denotes time differentiation and the Einstein convention for repeated indices is used.

The stress-strain relations for a Kelvin-Voigt solid are a simple generalization of those for one-dimensional media (Carcione, 2007):

$$\sigma_{ij} = \left(\lambda\theta + \lambda'\dot{\theta}\right)\cdot\delta_{ij} + 2\mu\varepsilon_{ij} + 2\mu'\dot{\varepsilon}_{ij}, \tag{2}$$

where λ and μ are the Lamé constants, λ' and μ' are the corresponding anelastic parameters,

$$\varepsilon_{ij} = \frac{1}{2}\left(\frac{\partial u_i}{\partial x_j} + \frac{\partial u_j}{\partial x_i}\right) \tag{3}$$

are the strain components,

$$\theta = \frac{\partial u_i}{\partial x_j}, \tag{4}$$

and δ_{ij} is Kronecker's delta.

2.2 Frequency domain analysis

In the frequency domain, equation (1) can be written as:

$$\sigma_{ij} = \mathbf{\Lambda}\theta\delta_{ij} + 2\mathbf{\Sigma}\varepsilon_{ij}, \tag{5}$$

where:

$$\mathbf{\Lambda} = \lambda + i\omega\lambda' \text{ and } \mathbf{\Sigma} = \mu + i\omega\mu' \tag{6}$$

are the complex Lamé moduli and ω is the angular frequency. Use of the correspondence principle allows the calculation of the phase velocity (v_p) and quality factor (Q) versus frequency:

$$v_p = \left[\mathrm{Re}\left(\frac{1}{v}\right)\right]^{-1} \tag{7}$$

and

$$Q = \frac{\mathrm{Re}(v^2)}{\mathrm{Im}(v^2)} \tag{8}$$

(Carcione, 2007), where v is either the P-wave complex velocity or the S-wave complex velocity, given by:

$$v(P) = \sqrt{\frac{\Lambda + 2\Sigma}{\rho}} \text{ and } v(S) = \sqrt{\frac{\Sigma}{\rho}}, \tag{9}$$

respectively. Re and Im take real and imaginary parts. The phase velocities of the P and S waves tend to $\sqrt{E/\rho}$ and $\sqrt{\mu/\rho}$ for $\omega \to 0$, and to ∞ for $\omega \to \infty$, where $E = \lambda + 2\mu$. The P- and S-wave quality factor are simply:

$$Q_P = \frac{E}{\omega E'} \quad \text{and} \quad Q_S = \frac{\mu}{\omega\mu'}, \tag{10}$$

where $E' = \lambda' + 2\mu'$. The attenuation factor is given by:

$$\alpha = \frac{\omega}{v_p}\left[\sqrt{1+Q^2} - Q\right] \tag{11}$$

(Carcione, 2007), where v_p and Q are the phase velocity and quality factor of the P wave or S wave. For low-loss media (Q>>1), equation (11) becomes:

$$\alpha(P)=\frac{\omega^2 E'}{2Ev_p} \quad \text{and} \quad \alpha(S)=\frac{\omega^2 \mu'}{2\mu v_p}, \tag{12}$$

where equations (10) have been used. Then, the attenuation factor is approximately proportional to the square of the frequency if the variation of the phase velocity is small over the range of frequencies of the signal.

The anelastic parameters can be obtained from the quality factors at a given frequency, say, the central frequency of the source, ω_0. We obtain:

$$\lambda'=\frac{1}{\omega_0}\left(\frac{E}{Q_{P0}}-\frac{2\mu}{Q_{S0}}\right) \text{ and } \quad \mu'=\frac{\mu}{\omega_0 Q_{S0}}, \tag{13}$$

where Q_{P0} and Q_{S0} are the quality factors at $\omega=\omega_0$, and E and μ are the moduli at ω=0.

The moduli can be obtained from the P- and S-wave phase velocities at $\omega=\omega_0$, $v_{p0}(P)$ and $v_{p0}(S)$, respectively. Using equations (6), (7), (9) and (10) gives

$$E=\rho v_{p0}^2(P)g(Q_{P0}) \quad \text{and} \quad \mu=\rho v_{p0}^2(S)g(Q_{S0}), \tag{14}$$

where:

$$g(a)=\frac{1}{2}\left(1+a^{-2}\right)^{-1/2}\left[1+\left(1+a^{-2}\right)^{-1/2}\right]. \tag{15}$$

Note that $g(a) \to 1$ when $a \to \infty$. Hence, the input properties to the modeling program are ρ, $v_{p0}(P)$, $v_{p0}(S)$, Q_{P0} and Q_{S0}.

2.3 Velocity-stress formulation

Introducing the particle-velocity components, $v_i=\dot{u}_i$ the equations of momentum conservation (1) become:

$$\dot{v}_i=\frac{1}{\rho}\frac{\partial \sigma_{ij}}{\partial x_j}. \tag{16}$$

Using equations (3) and (4), the time derivative of the stress-strain relations (2) become:

$$\dot{\sigma}_{ij} = \left(\lambda \frac{\partial v_i}{\partial x_i} + \lambda' \frac{\partial \dot{v}_i}{\partial x_i} \right) \delta_{ij} + \mu \left(\frac{\partial v_i}{\partial x_j} + \frac{\partial v_j}{\partial x_i} \right) + \mu' \left(\frac{\partial \dot{v}_i}{\partial x_j} + \frac{\partial \dot{v}_j}{\partial x_i} \right) + \dot{m}_{ij} \quad (17)$$

where m_{ij} are moment-tensor components per unit volume defining the strength and radiation pattern of the source mechanism. Substituting (16) into (17) yields:

$$\dot{\sigma}_{ij} = \lambda \frac{\partial v_i}{\partial x_i} \delta_{ij} + \lambda' \left[\frac{\partial}{\partial x_i} \left(\frac{1}{\rho} \frac{\partial \sigma_{ij}}{\partial x_j} \right) \right] \delta_{ij} + \mu \left(\frac{\partial v_i}{\partial x_j} + \frac{\partial v_j}{\partial x_i} \right) +$$

$$+ \mu' \left[\frac{\partial}{\partial x_j} \left(\frac{1}{\rho} \frac{\partial \sigma_{im}}{\partial x_m} \right) + \frac{\partial}{\partial x_i} \left(\frac{1}{\rho} \frac{\partial \sigma_{jm}}{\partial x_m} \right) \right] + \dot{m}_{ij} \, . \quad (18)$$

Let us express the velocity-stress formulation in explicit form. Define the quantities:

$$\prod_x = \frac{1}{\rho} \left(\frac{\partial \sigma_{xx}}{\partial x} + \frac{\partial \sigma_{xy}}{\partial y} + \frac{\partial \sigma_{xz}}{\partial z} \right),$$

$$\prod_y = \frac{1}{\rho} \left(\frac{\partial \sigma_{xy}}{\partial x} + \frac{\partial \sigma_{yy}}{\partial y} + \frac{\partial \sigma_{yz}}{\partial z} \right), \quad (19)$$

$$\prod_z = \frac{1}{\rho} \left(\frac{\partial \sigma_{xz}}{\partial x} + \frac{\partial \sigma_{yz}}{\partial y} + \frac{\partial \sigma_{zz}}{\partial z} \right),$$

$$\psi = \frac{\partial \prod_x}{\partial x} + \frac{\partial \prod_y}{\partial y} + \frac{\partial \prod_z}{\partial z} \quad (20)$$

and

$$\vartheta = \dot{\theta} = \frac{\partial v_x}{\partial x} + \frac{\partial v_y}{\partial y} + \frac{\partial v_z}{\partial z} \, . \quad (21)$$

Then, equations (16) and (18) can be written in components as:

$$\dot{v}_x = \prod_x, \quad \dot{v}_y = \prod_y, \quad \dot{v}_x = \prod_x,$$

$$\dot{\sigma}_{xx} = \lambda\vartheta + \lambda'\psi + 2\mu\frac{\partial v_x}{\partial x} + 2\mu'\frac{\partial \prod_x}{\partial x} + \dot{m}_{xx},$$

$$\dot{\sigma}_{yy} = \lambda\vartheta + \lambda'\psi + 2\mu\frac{\partial v_y}{\partial y} + 2\mu'\frac{\partial \prod_y}{\partial y} + \dot{m}_{yy},$$

$$\dot{\sigma}_{zz} = \lambda\vartheta + \lambda'\psi + 2\mu\frac{\partial v_z}{\partial z} + 2\mu'\frac{\partial \prod_z}{\partial z} + \dot{m}_{zz}, \qquad (22)$$

$$\dot{\sigma}_{xy} = \mu\left(\frac{\partial v_x}{\partial y} + \frac{\partial v_y}{\partial x}\right) + \mu'\left(\frac{\partial \prod_x}{\partial y} + \frac{\partial \prod_y}{\partial x}\right) + \dot{m}_{xy},$$

$$\dot{\sigma}_{xz} = \mu\left(\frac{\partial v_x}{\partial z} + \frac{\partial v_z}{\partial x}\right) + \mu'\left(\frac{\partial \prod_x}{\partial z} + \frac{\partial \prod_z}{\partial x}\right) + \dot{m}_{xz},$$

$$\dot{\sigma}_{yz} = \mu\left(\frac{\partial v_x}{\partial z} + \frac{\partial v_z}{\partial x}\right) + \mu'\left(\frac{\partial \prod_y}{\partial z} + \frac{\partial \prod_z}{\partial y}\right) + \dot{m}_{yz}.$$

Equations (19) and (22) constitute the velocity-stress formulation for the Kelvin-Voigt model. The model requires three arrays for the particle-velocity components, six arrays for the stress-tensor components, and four arrays for the material properties. On the other hand, the equation of motion based on a single Zener model requires six additional arrays for the memory variables and two additional arrays for the material properties. The extra cost to avoid these memory requirements is the calculation of the nine additional spatial derivatives corresponding to the acceleration components.

2.4 The numerical algorithm

The numerical solution is obtained by using a 4th-order Runge-Kutta method as time-stepping algorithm, the Chebyshev differential operator to compute the spatial derivatives along the vertical direction, and the Fourier differential operator along the horizontal directions.

The Fourier and Chebyshev methods (Carcione, 1992; Carcione, 2007), consist of a spatial discretization and calculation of spatial derivatives using the fast Fourier transform. The Fourier method is a collocation technique in which a continuous function is approximated by a truncated series of trigonometric functions, wherein the spectral (expansion) coefficients are chosen such that the approximate solution coincides with the exact solution at the discrete set of sampling or collocation points. The

collocation points are defined by equidistant sampling points. Since the expansion functions are periodic, the Fourier method is appropriate for problems with periodic boundary conditions. In the Chebyshev method, the collocation points are the roots of the Chebyshev polynomials. It is appropriate for simulating Neumann and Dirichlet boundary conditions. The Fourier and Chebyshev methods are infinitely accurate up to the maximum wavenumber of the mesh, that corresponds to a spatial wavelength of two grid points (at maximum grid spacing for the Chebyshev operator).

The conventional Chebyshev method has two major disadvantages. In the first place, the grid points are restricted to the Gauss-Lobatto collocation points. This poses a limitation regarding the location of the interfaces. Secondly, the clustering of grid points at the ends of the mesh restricts the time step of the time integration scheme, which has to be of the order $O(N^{-2})$ where N is the number of grid points. Here, we use a mapping transformation for the vertical coordinate, which circumvents the severe stability condition of the integration method and distribute grid points in arbitrary locations.

By stretching the mesh, we increase the minimum grid spacing and are able to increase the time step of the Runge-Kutta algorithm, thus reducing the computer time. For this purpose we have implemented the stretching function and algorithm described by Kosloff and Tal-Ezer (1993) who claim to obtain time steps of the order $O(N^{-1})$.

Furthermore, this transformation can be used for spatial grid adaptation (Augenbaum (1989), Bayliss *et al.* (1995), Guillard *et al.* (1992)) in the sense that the collocation points can be redistributed and properly concentrated in regions with steep velocity gradients, fine layering and complex interface geometries. Similar mapping transformations can be applied in the horizontal directions, where the Fourier differential operator is used (Fornberg, 1988).

In particular the time step depends on the size of the first grid cell at the end of the mesh. In general, stability can be achieved with the condition satisfied by the Fourier method. For the Runge-Kutta method the condition is $v \cdot dt/dz < 2.79$ (Jain, 1984), where v is the maximum wave velocity, dt is the time step and dz is the minimum grid spacing.

Boundary conditions are implemented by using a boundary treatment based on characteristics variables (Kosloff *et al.*, 1990). This method has been proposed by Bayliss *et al.* (1986) to model free surface and non-reflecting boundary conditions. The wave equation is decomposed into outgoing and incoming wave modes perpendicular to the free surface. The

outgoing waves are determined by the solution inside the domain, while the incoming waves are calculated from the boundary conditions.

In addition to the non-reflecting conditions, absorbing strips are used to further attenuate the wave field at the bottom of the mesh (Kosloff and Kosloff, 1986). This combined use of damping methods practically eliminates any wraparound caused by the Fourier operator at the boundaries of the mesh.

2.5 The moment tensor

Following Aki and Richards (1980) the radiation pattern of the source can be described with the moment tensor. The different components of the moment tensor are computed as a function of the fault mechanism (angles of strike, dip and rake):

$$
\begin{aligned}
M_{xx} &= -M_0(\sin\delta\cos\lambda\sin 2\phi + \sin 2\delta\sin\lambda\sin^2\phi)\,,\\
M_{xy} &= M_0(\sin\delta\cos\lambda\sin 2\phi + \frac{1}{2}\sin 2\delta\sin\lambda\sin 2\phi)\,,\\
M_{xz} &= -M_0(\cos\delta\cos\lambda\cos\phi + \cos 2\delta\sin\lambda\sin\phi)\,,\\
M_{yy} &= M_0(\sin\delta\cos\lambda\sin 2\phi - \sin 2\delta\sin\lambda\cos^2\phi)\,,\\
M_{yz} &= -M_0(\cos\delta\cos\lambda\sin\phi - \cos 2\delta\sin\lambda\cos\phi)\,,\\
M_{zz} &= M_0\sin 2\delta\sin\lambda\,,
\end{aligned}
\tag{23}
$$

where M_0 is the seismic moment and ϕ, δ and λ are the angles of strike, dip and rake, respectively.

2.6 Source implementation

The seismological source is defined following the work of Pitarka (1999). The moment-tensor formulation considers source stress components m_{ij} appropriately added to the stresses at the grid point corresponding to the source location. They are given by:

$$m_{ij} = M_{ij}\dot{m}(t)/V\,, \tag{25}$$

where M_{ij} are the moment tensor components and $\dot{m}(t)$ is a normalized source time history satisfying the relation:

$$\int_{t_0}^{t_f}\dot{m}(t)dt = 1\,. \tag{26}$$

V is the effective volume of the grid cell in which the source is located:

$$V = dx \cdot dy \cdot dz \tag{27}$$

if the grid is uniform,

$$V = \frac{(dx_i - dx_{i-1})}{2} \cdot \frac{(dy_i - dy_{i-1})}{2} \cdot \frac{(dz_i - dz_{i-1})}{2} \tag{28}$$

if the grid spacing is not uniform.

The time history is a bell-shaped time function given by:

$$\dot{m}(t) = \left[1 - \cos(2\pi\, t / T_0)\right] / T_0 \,, \tag{29}$$

where T_0 is the duration time.

3. MESSINA 1908 EARTHQUAKE NUMERICAL SIMULATION

A well known geological model consists of sub-horizontal layers, with the seismic properties of the different layers given in Table 1. The focal mechanism is described in Table 2 and Figure 2 shows the location map of the study area.

Table 1: Seismic properties of the layers for the geological model of the 1908 Messina earthquake simulation.

Layer	Depth	Density	v_{p0}(P)	Q_P	v_{p0}(S)	Q_S
	(m)	*(kg/m^3)*	*(m/s)*		*(m/s)*	
1	0	1940	2200	10	400	20
2	25	1940	1900	10	400	20
3	56	1940	2050	10	400	20
4	99	2000	3300	20	1000	20
5	153	2000	3300	20	1350	20
6	219	2000	2700	10	650	20
7	382	2000	2900	20	1000	20
8	477	2450	3000	20	1700	10
9	1996	2600	4600	60	2690	30
10	5981	2650	5900	60	3450	30
11	14910	2700	6550	60	3850	30
12	19924	2900	7600	60	4450	30

13	26258	3200	8000	60	4680	30

Table 2: Parameters of the fault constituting the source for 1908 Messina earthquake simulation.

Strike	20°
Dip	29°
Rake	270°
Depth	3-12.7 km
M_0	$7 \cdot 10^{19}$ Nm

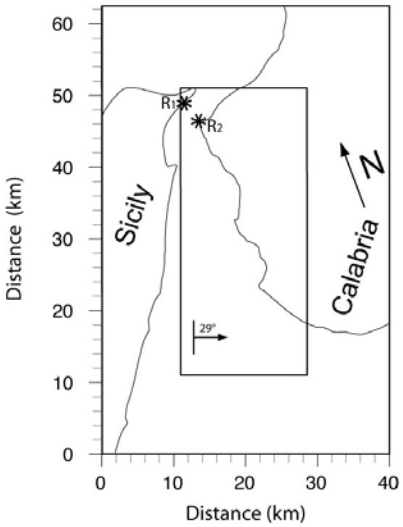

Figure 2: Location map of the study area. The inner rectangle represents the plan view of the seismogenic fault. R1 and R2 are the locations of two receivers whose seismograms are given in Figure 4.

The seismic moment is uniformly distributed over a fault plane having the longer edges parallel to the earth surface (Figure 2). Receivers are located at the surface and at coordinates x = 49 km, y = 11.5 km for R1 and x = 46.5 km, y = 13.5 km for R2.

The numerical mesh has 80 x 125 x 136 grid points with a grid spacing of 500 m in the x- and y-directions. The grid spacing in the z-direction varies between 5.6 and 215 m. The Chebyshev method used to solve spatial derivatives in the vertical direction has the grid points in the positions defined by the Gauss-Lobatto collocation points. The dimensions

of the geological model are 40 x 62.5 x 29.19 km.

The wavefield is computed by using a time step of 5 ms. The source time history is given in equation (29) with a duration time T_0 of 1 s.

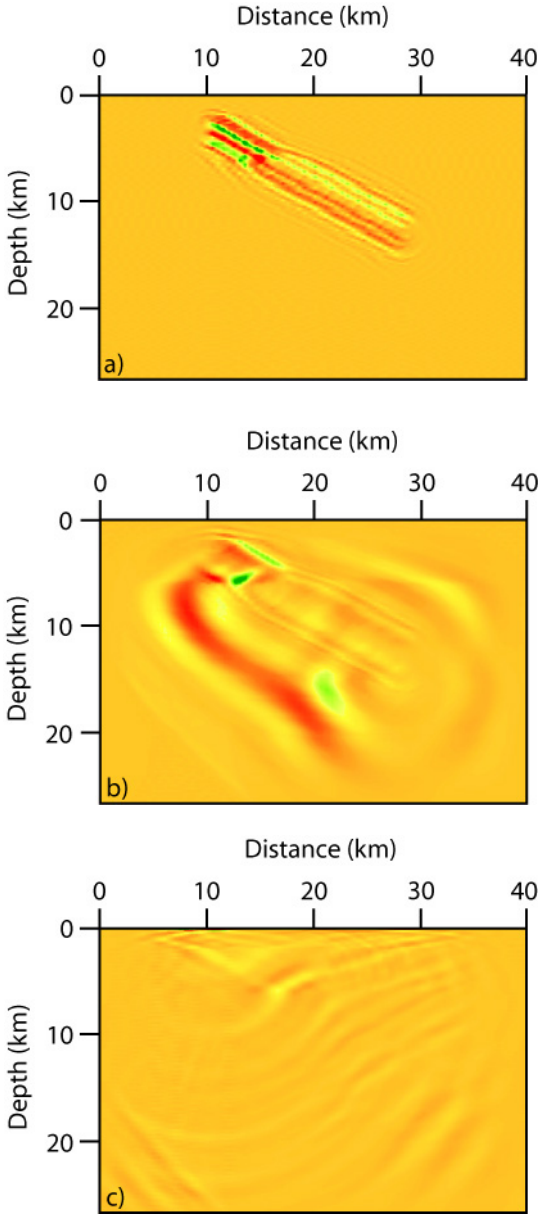

Figure 3: Snapshots of the vertical component of the velocity field at 0.8 s (a), 3.2 s (b), and 8.0 s (c) along a vertical plane parallel to the shorter dimension of the fault.

Snapshots of the vertical component of the velocity field are given in Figure 3 at 0.8, 3.2 and 8.0 s. The velocity field is recorded in a vertical plane parallel to the shorter dimension of the fault. Figure 4 shows the three component of the normalized seismograms recorded at the two stations R1 and R2.

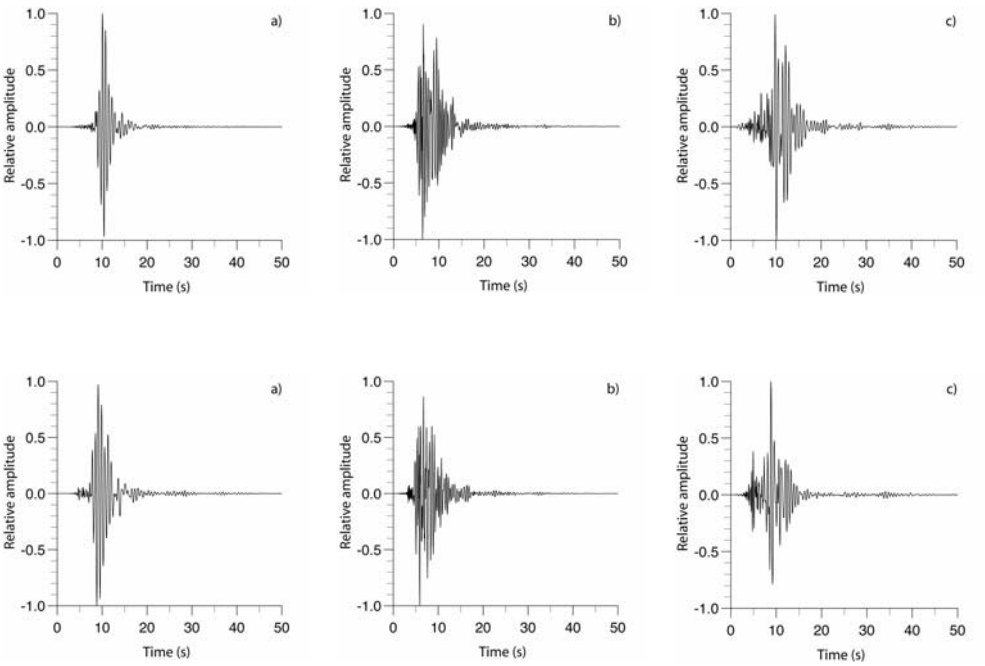

Figure 4: Seismograms of the particle velocity (normalized) recorded at the Sicilian and Calabrian coasts (upper and lower plots, respectively); (a), (b) and (c) correspond to Vx, Vy and Vz, respectively.

4. CONCLUSIONS

We have developed a numerical approach for wave simulation in anelastic media in the presence of free surface. The modelling simulates 3-D waves by using the Fourier and Chebyshev methods to compute the spatial

derivatives along the horizontal and vertical directions, respectively. The stress-strain relation is based on the Kelvin-Voigt mechanical model. We have used the developed algorithm to simulate the 1908 Messina Earthquake.

References

Aki K., Richards P. G. (1980) *Quantitative seismology, theory and methods*, Vol. 1, W. H Freeman and Company.

Amoruso A., Crescentini L., Scarpa R. (2002) Source parameters of the 1908 Messina Straits, Italy, earthquake from geodetic and seismic data, *Journal of Geophysical Research*, **107**, NO. B4, 10.1029/2001JB000434.

Augenbaum J. M. (1989) An adaptive pseudospectral method for discontinuous problems, *Appl. Num. Math.*, **5**, pp. 459-480.

Bayliss A., Class A., Matkowsky B. J. (1995) Adaptive approximation of solutions to problems with multiple layers by Chebyshev pseudo-spectral methods, *J. Comput. Phys*., **116**, pp. 160-172.

Bayliss A., Jordan K.E., LeMesurier B.J., Turkel E. (1986) A fourth-order accurate finite difference scheme for the computation of elastic waves, *Bull. Seism. Soc. Am.*, **76**, 1115-1132.

Baratta M. (1910) La catastrofe sismica Calabro-Messinese (28 dicembre 1908), *Rel. Soc. Geogr. It.*, Roma, 496.

Boschi E., Pantosti D., Valensise L. (1989) Modello di sorgente per il terremoto di Messina del 1908 ed evoluzione recente dell'area dello Stretto, *Atti dell'VIII convegno del G.N.G.T.S.*, Roma, 245-258.

Capuano P., De Natale G., Gasparini P., Pingue F., Scarpa R. (1988) A model for the 1908 Messina Straits (Italy) earthquake by inversion of levelling data, *Bullettin of the Seism. Soc. of America*, **78**(6), 1930-1947.

Carcione J. M. (1992) Modeling anelastic singular surface waves in the Earth, *Geophysics*, **57**, 781-792.

Carcione J.M. (2007) *Wave Fields in Real Media. Theory and numerical simulation of wave propagation in anisotropic, anelastic, porous and electromagnetic media*, Elsevier. (2nd edition, revised and extended).

Carcione J.M., Herman G., ten Kroode F. P. E. (2002) Seismic modeling, *Geophysics*, **67**, 1304-1325.

Fornberg B. (1988) The pseudospectral method: accurate representation of interfaces in elastic wave calculations, *Geophysics*, **53**, 625-637.

Guillard H., Malè J. M., Peyret R. (1992) Adaptive spectral methods with application to mixing layer computation, *J. Comput. Phys*., **102**, 114-127.

Gutemberg, B., Richter C. F. (1954) *Seismicity of the Earth and associated phenomena*, II edition, Princeton University Press, Princeton, New Jersey.

Jain M. K. (1984) *Numerical solutions of differential equations*, Wiley Eastern Ltd.

Kosloff D., Kessler D., Filho A. O., Tessmer E., Behle A., Strahilevitz R. (1990) Solution of the equation of dynamic elasticity by a Chebychev spectral method, *Geophysics*, **55**, 734-748.

Kosloff D., Kosloff R. (1986) Absorbing boundaries for wave propagation problems, *J. Comput. Phys*., **63**, 363-376.

Kosloff, D., Tal-Ezer H. (1993) A modified Chebyshev pseudospectral method with an *O(N-1)* time step restriction, *J. Comp. Phys*., **104**, 457-469.

Mercalli G. (1909) Contributo allo studio del terrmoto calabro-messinese del 28 dicembre 1908, *Atti R. Ist. Incoraggiamento di Napoli*, VI – 7.

Mulargia F., Boschi E. (1983) The 1908 Messina earthquake and related seismicity, *Proceeding of the International School of Physics Enrico Fermi*, Course LXXXV, 493-518.

Pitarka A. (1999) Elastic finite-difference modeling of seismic motion using staggered grids with non uniform spacing, *Bull. Seis. Soc. Am.*, **89**(1), 54 – 68.

Platania G. (1909) Il maremoto dello Stretto di Messina del 28 Dicembre 1908, *Boll. Sismol. Soc. It.*, **22**, 369-458.

Riuscetti M., Schick R. (1975) Earthquakes and tectonics in Southern Italy, *Boll. Geof. Teor. Appl.*, **17**, 59-78.